Supporting information

Self-Assembly of a Giant Molybdenum Titanium-oxo Cluster [Mo$_{42}$Ti$_{12}$(O$_2$)$_{24}$] for Bifunctional Oxidation Catalysis

Ming Xu,[a] Ting Wang,*[a] Wenjing Zhang,[a] Keke Guo,[b] Ping Wang,[a] Chao Qin,[b] Lin Xu,[b] Zhongmin Su,[b] and Xinlong Wang*[b]

[a] Key Laboratory of Functional Materials Physics and Chemistry of the Ministry of Education, Jilin Normal University, Changchun, Jilin 130103

[b] Key Laboratory of Polyoxometalate and Reticular Material Chemistry of Ministry of Education Northeast Normal University, Changchun, Jilin 130024

*Corresponding Authors: wangt@jlnu.edu.cn; wangxl824@nenu.edu.cn

Contents

Section S1 Experimental Methods

Section S2 Supplementary Figures

Section S3 Supplementary Tables

Section S4 References

Section S1 Experimental Methods

1.1 Materials and General Methods

All commercially obtained reagents, including $(NH_4)_6Mo_7O_{24} \cdot 4H_2O$, $TiCl_4$, H_2O_2, KOH, and HCl were purchased from Aldrich and used without further purification. Elemental analyses (Ti, Mo, K) were performed on a PLASMA-SPEC (I) ICP atomic emission spectrometer. Thermogravimetric analysis (TGA) of the samples was performed using a Perkin-Elmer TG-7 analyzer heated from room temperature to 800 °C under nitrogen at the heating rate of 10 °C min^{-1}. FT/IR spectrum was performed in the range 4000-400 cm^{-1} using KBr pellets on an Alpha Centaurt FT/IR spectrophotometer. The surface photovoltage (SPV) spectroscopy was carried out on a lab-made instrument, which constitutes a source of monochromatic light, a lock-in amplifier (SR830-DSP) with a light chopper (SR540). Diffuse reflectance UV-vis spectra were measured from 200 to 600 nm on a Varian Cary 500 UV-vis NIR spectrometer equipped with a 110 mm diameter integrating sphere at room temperature. A barium sulfate ($BaSO_4$) pellet was used as the standard with 100% reflectance. Energy dispersive X-ray (EDX) spectra and elemental mapping were obtained from a JEOL JSM 4800 F scanning electron microscope. The photocurrent (*I-t*) and Mott-Schottky curves were recorded in the CHI660c electrochemistry station with Xenon lamp as the light source under ambient conditions.

1.2 X-ray Crystallography

The data collections was performed on a Bruker D8-Venture diffractometer with a Turbo X-ray Source (Mo Kα radiation, λ = 0.71073 Å) adopting the direct drive rotating anode technique and a CMOS detector at 173 K. The data frames were collected using the program APEX-3 and processed using the program SAINT routine in APEX-3. The structure was solved by direct method and refined by the full-matrix least-squares on F^2 using the SHELXL-2014 program.[1] The diffused electron densities resulting from these residual solvent molecules were removed from the data set using the SQUEEZE[2] routine of PLATON[3] and refined further using the data generated. The restrained SIMU, SADI instructions were used to make the structures more reasonable. The formula unit was obtained through a combination of elemental analyses and thermogravimetric characterization. Deposition Number CSD: 2068105 contains the supplementary crystallographic data for this paper. These data are provided free of charge by the joint Cambridge Crystallographic Data Centre and Fachinformationszentrum Karlsruhe Access Structures service www.ccdc.cam.ac.uk/structures.

1.3 Bond valence sum (BVS) analysis:

The BVS values (Vi) of titanium and molybdenum atoms in 1 were calculated using the following equation:[4,5]

$$V_i = \sum \exp\left(\frac{r_o - r_{ij}}{B}\right)$$

where ro and rij are the bond valence parameter and the bond length between atoms i and j, respectively, while B is a constant value of 0.37 Å.
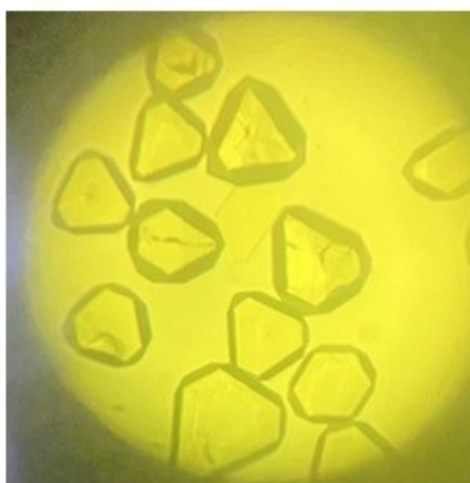
Section S2 Supplementary Figures

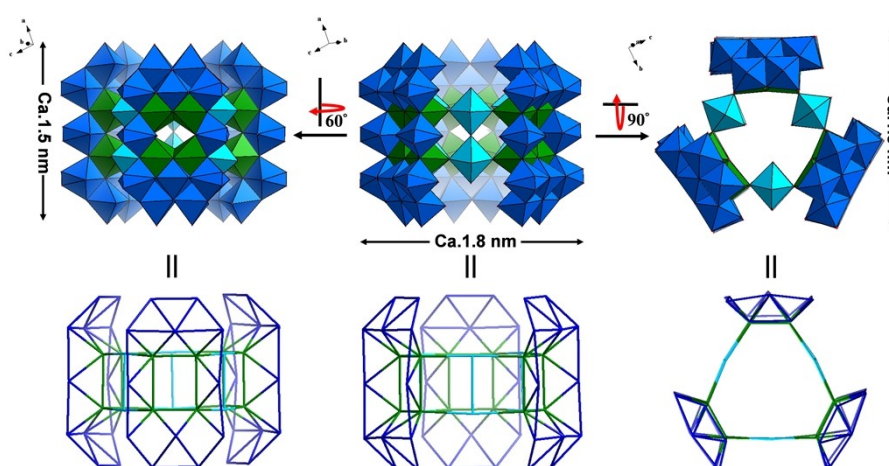**Figure S1.** The crystal of **1** under an optical microscope.

Figure S2. The polyhedron and metal-based skeleton conversions of **1** with different perspectives. Color codes: MoO_6/MoO_7 polyhedra, blue/sky blue; TiO_7 polyhedra, green.
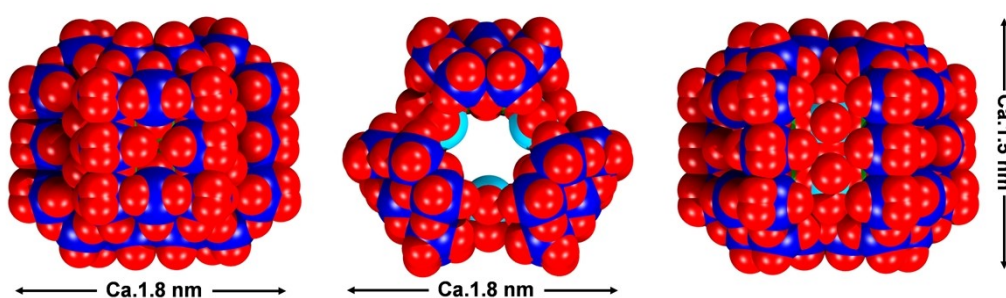

Figure S3. The structure of **1** viewed along with different perspectives in space-filling mode.
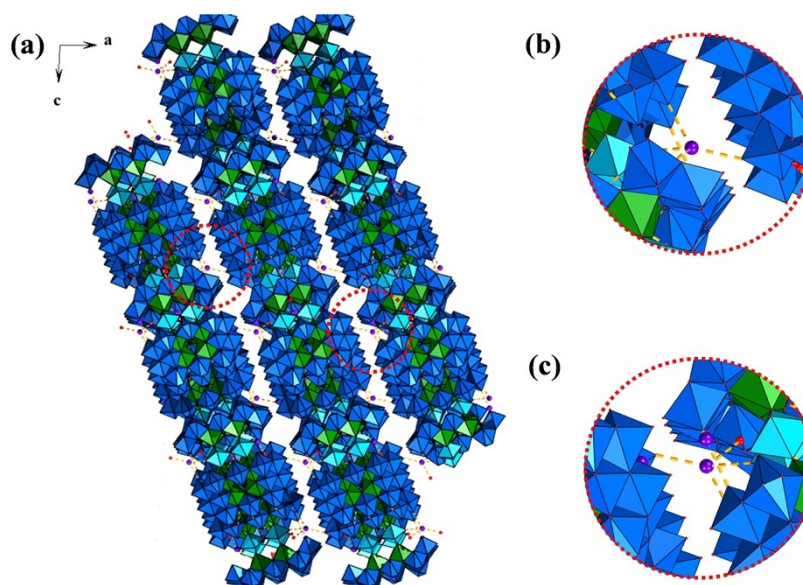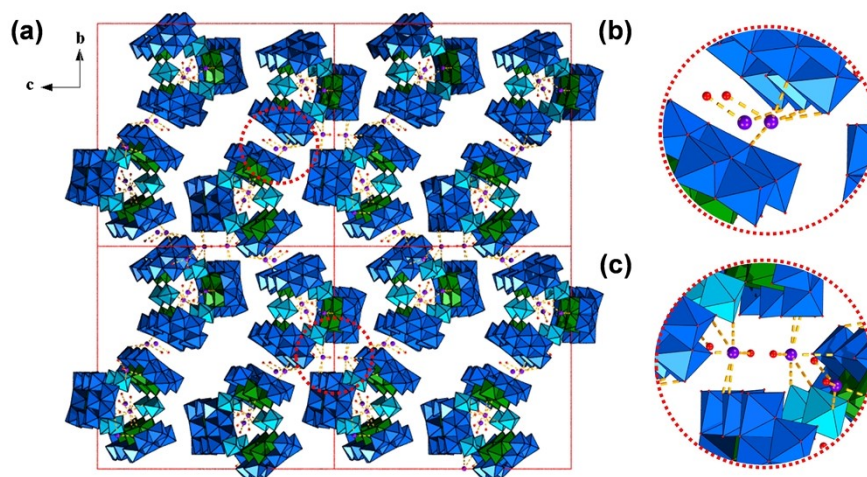
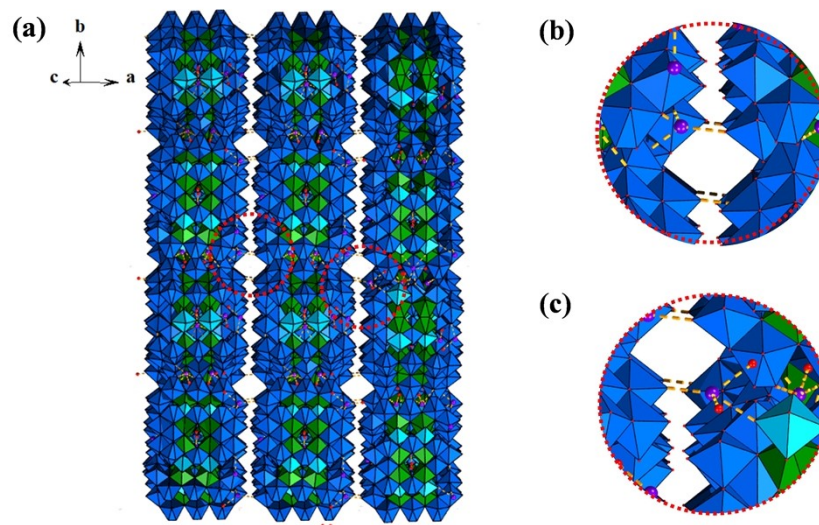**Figure S4.** The three-dimensional supramolecular packing along the a-axis of **1**.

Figure S5. The three-dimensional supramolecular packing along the b-axis of **1**.

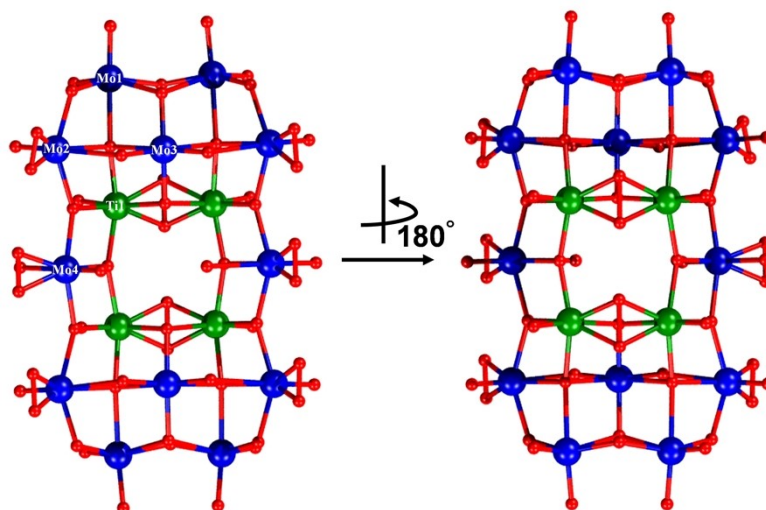**Figure S6.** The three-dimensional supramolecular packing along the c-axis of **1**.

Figure S7. Ball-and-stick views of the {$Mo_{12}Ti_4$} building blocks with different perspectives. Color code: blue ball, Mo; green ball, Ti; red ball, O.
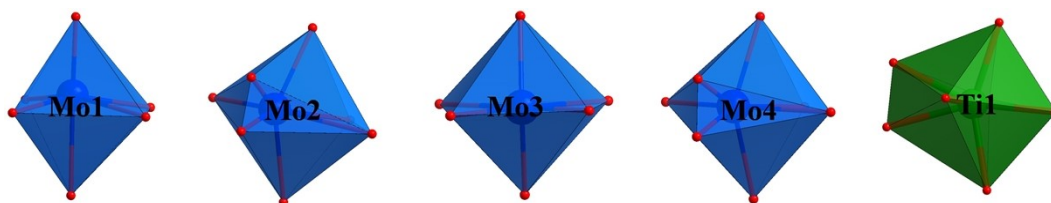

Figure S8. View of the detailed coordination configuration of Mo-O and Ti-O in polyhedron. Color codes: Mo-O polyhedra, blue; Ti-O polyhedra, green.
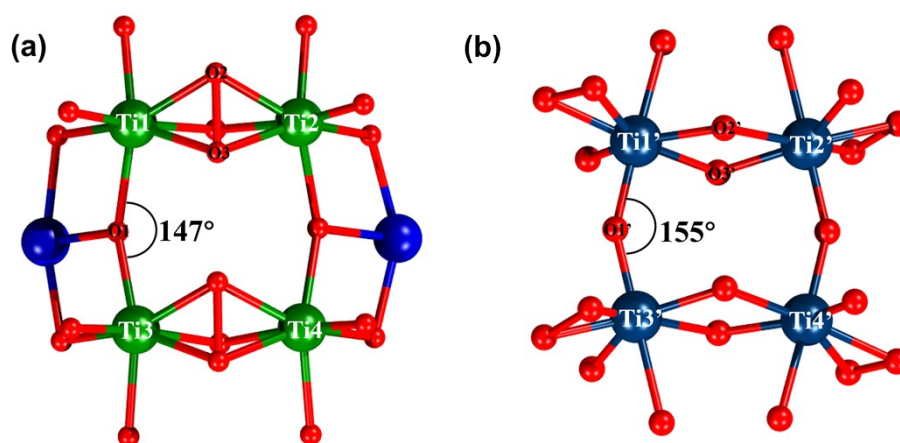

Figure S9. View of the different coordination modes of Ti ions in the reported (a) **1** and (b) {Ti_4-1}.

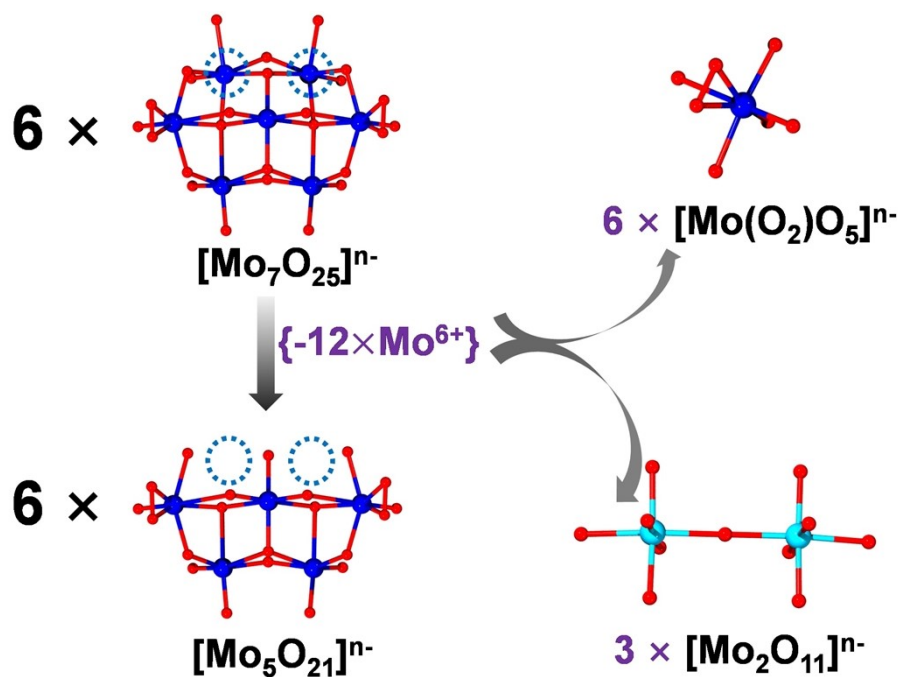**Figure S10.** Ball-and-stick views of the $[Mo_7O_{25}]^{n-}$ degraded into $[Mo_5O_{21}]^{n-}$ building blocks. Color code: blue ball, Mo; green ball, Ti; red ball. O.

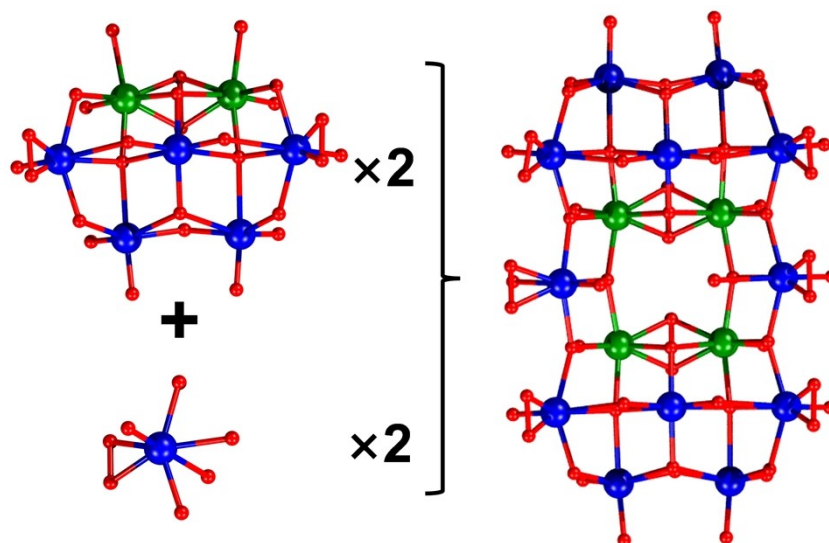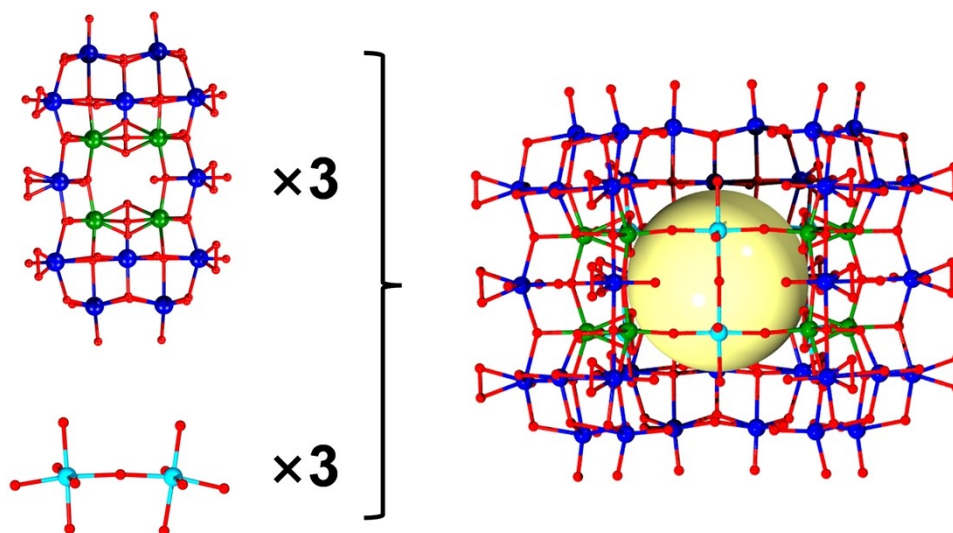**Figure S11.** Ball-and-stick views of the formation of $\{Mo_{12}Ti_4\}$. Color code: blue ball, Mo; green ball, Ti; red ball, O.

Figure S12. Ball-and-stick views of the formation of $\{Mo_{42}Ti_{12}\}$. Color codes: Color code: blue ball, Mo; green ball, Ti; red ball. O.
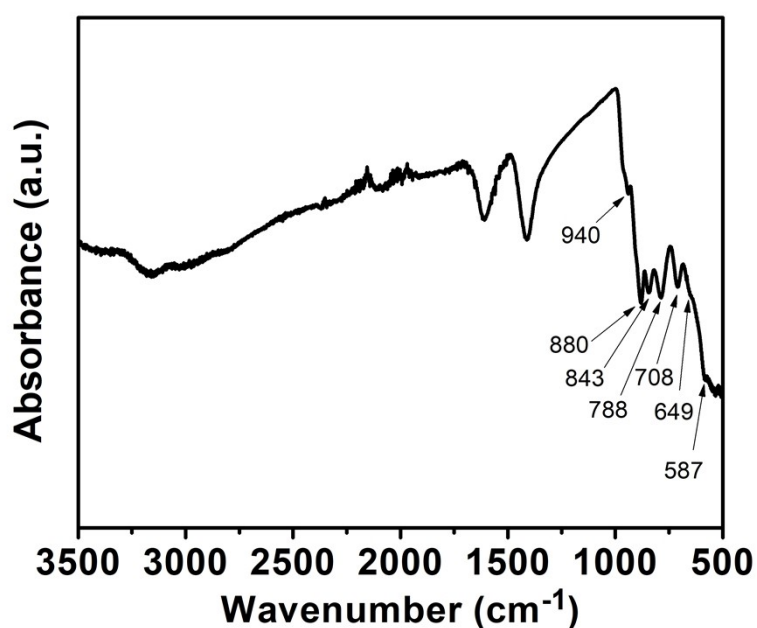
Figure S13. The FT-IR spectrum of **1**. The peaks at 940 cm^{-1}, 843 cm^{-1}, and 788 cm^{-1} may be assigned to stretching vibrations of terminal Mo=O bands, antisymmetric stretching vibrations of Mo-O-Mo bridges, and bending vibrations of Mo-O-Mo bridges, respectively. The peaks at 708 cm^{-1} and 649 cm^{-1} are assigned to the bending vibrations of Ti-O-Ti bridges and there is also a tiny peak at about 587 cm^{-1}, which is attributed to the presence of antisymmetric stretching vibrations Ti-O-Ti bridges.[6-8]
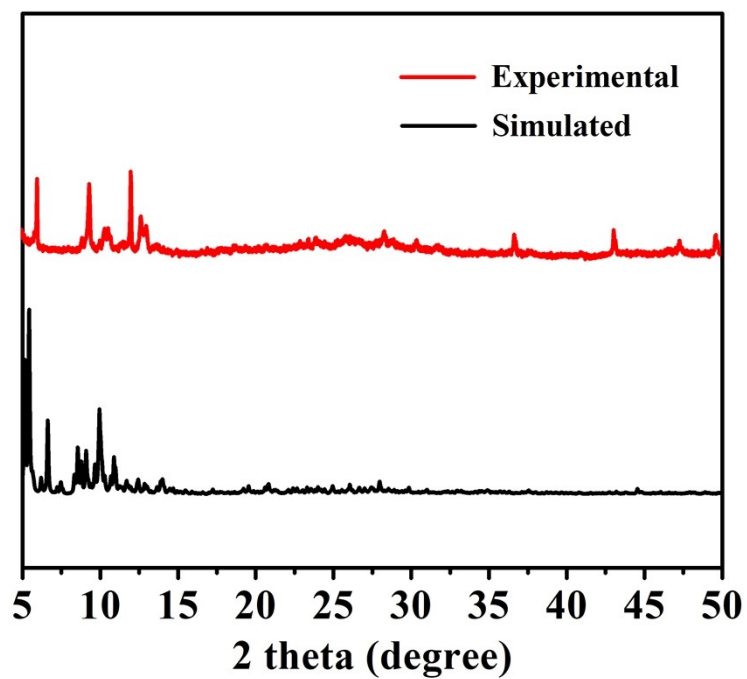
Figure S14. Simulated and experimental PXRD patterns of **1**.
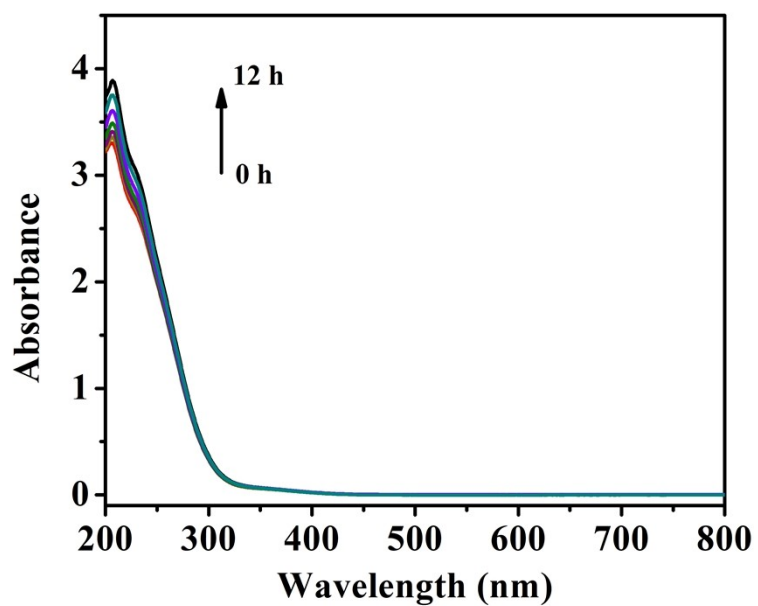
Figure S15. UV−vis absorption spectra of **1** in H_2O. UV−vis absorption spectra of **1** in aqueous solution exhibit consistent absorptions at about 206 nm, and their absorption profiles remain almost unchanged for 12 hours, confirming the good stability of **1** in H_2O.
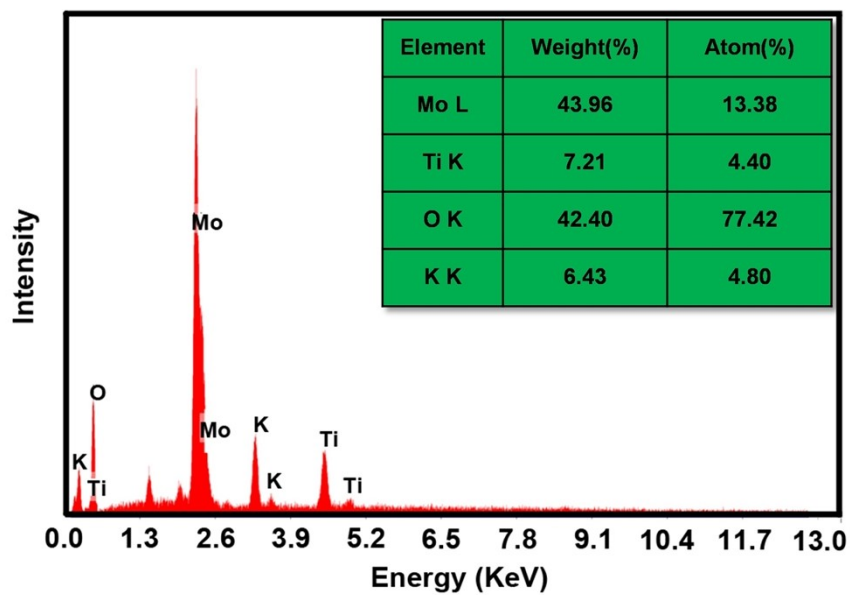
Figure S16. The EDX spectrum of **1**. The Mo, Ti, O and K elements are contained in **1**.
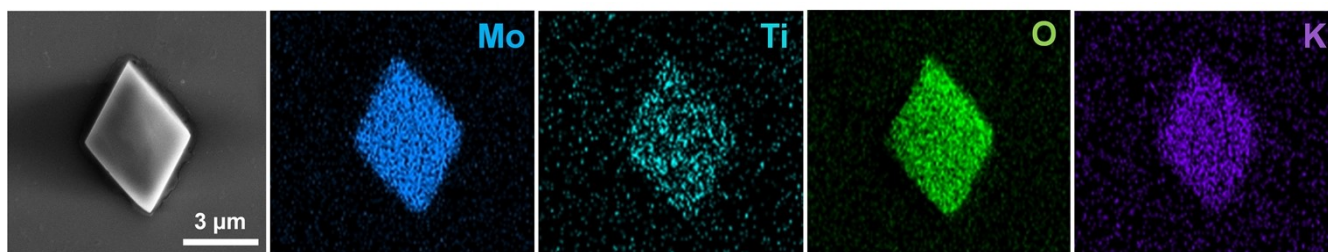
Figure S17. Elemental mapping of Mo, Ti, O and K in **1**.
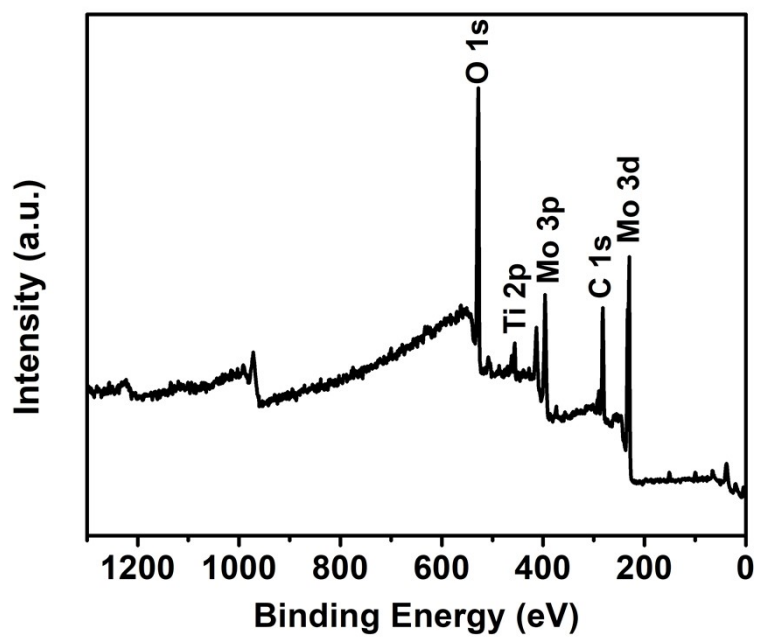
Figure S18. The full-scan X-ray photoelectron spectrum (XPS) spectra of **1**.
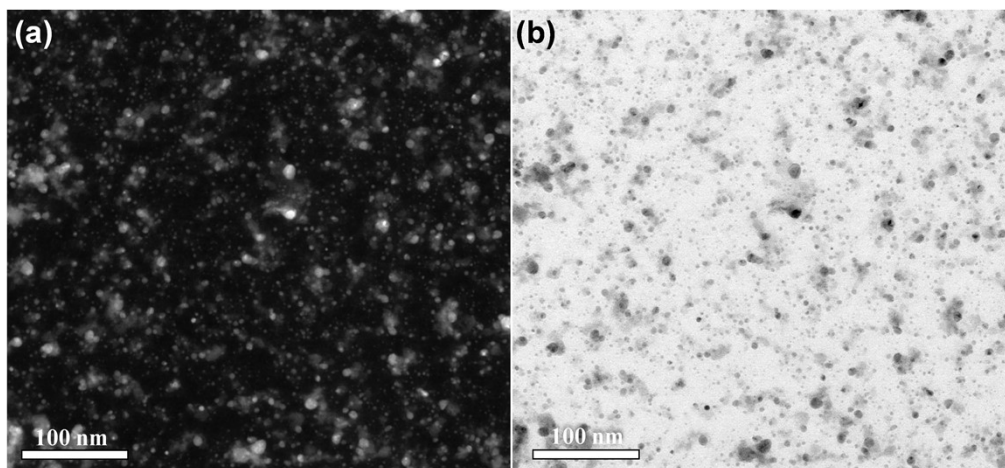
Figure S19. Dark-field STEM of **1**.
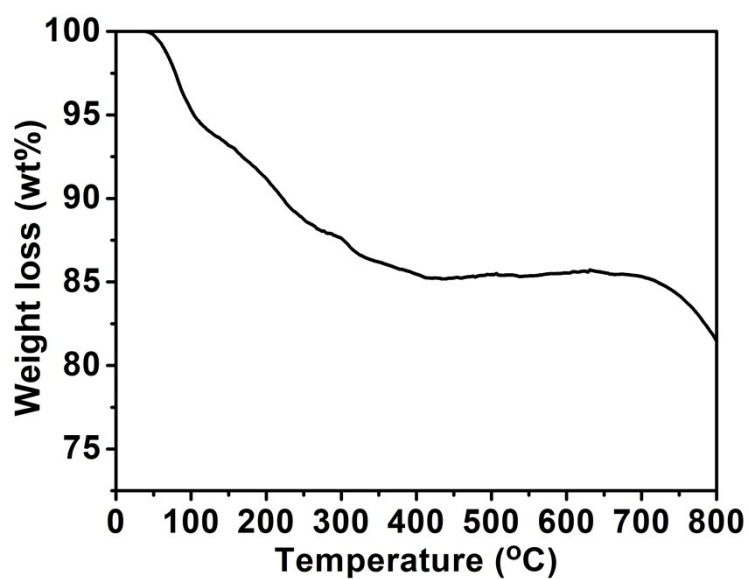
Figure S20. The TG curve of **1**.The TG curve exhibits that the weight loss of 6.9% at 25-150 °C and 5.3% at 150-278 °C correspond to the loss of crystalline water and coordination water in **1**, respectively, thus indicating the number of crystalline water in **1** is 31 and the structure of **1** can be maintained up to 275 °C.
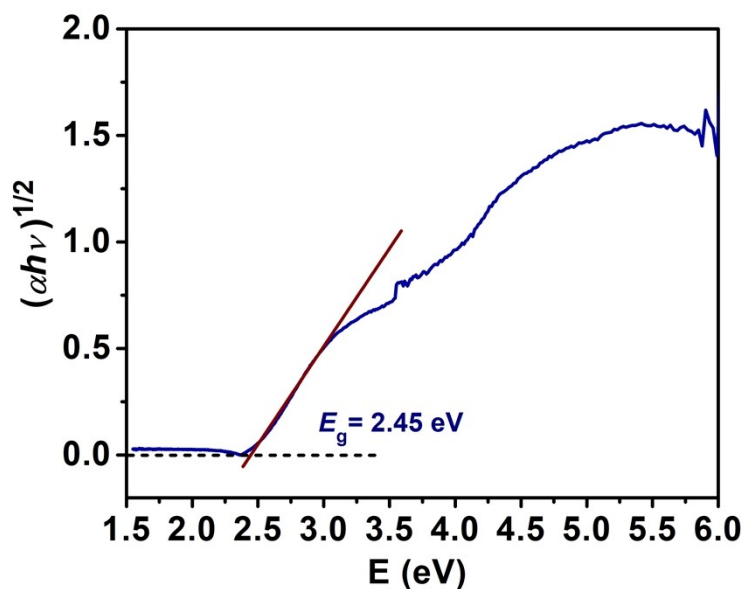
Figure S21. The plot of the Tauc's plot of the absorption spectra of **1**.
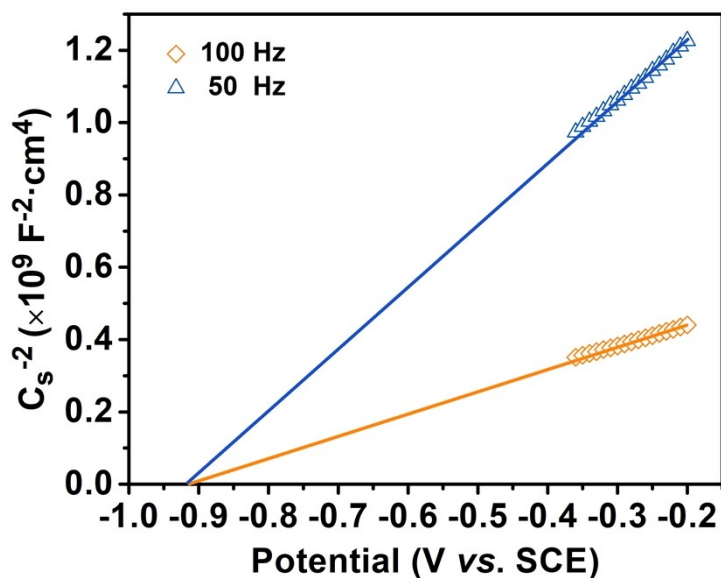
Figure S22. The Mott-Schottky curves of **1**. The Mott-Schottky curves show that the slopes in the linear region are positive, which indicates that **1** is an n-type semiconductor.
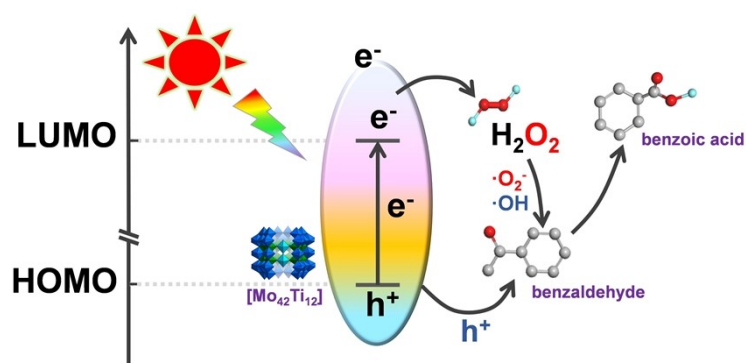
Figure S23. The reaction mechanism of photocatalytic benzaldehyde.

$$H_2O_2 \xrightarrow{h\nu} 2\cdot OH$$

$$\cdot OH + H_2O_2 \longrightarrow \cdot OOH + H_2O$$

$$\cdot OH + \cdot OOH \longrightarrow O_2 + H_2O$$

$$Mo_{42}Ti_{12} \xrightarrow{h\nu} Mo_{42}Ti_{12}(h_{VB}^+ + e_{CB}^-)$$

$$e_{CB}^- + O_2 \longrightarrow \cdot O_2$$

$$C_6H_5CHO + \cdot O_2(\cdot OH, h_{VB}^+) \longrightarrow C_6H_5COOH$$

Figure S24. The reaction mechanism of photocatalytic benzaldehyde.

Figure S25. The FT-IR spectra of **1** before and after catalytic reaction.

Figure S26. The XRD patterns of **1** before and after catalytic reaction.

Section S3 Supplementary Tables

Table S1. Collected Examples of molybdenum titanium-oxo clusters.

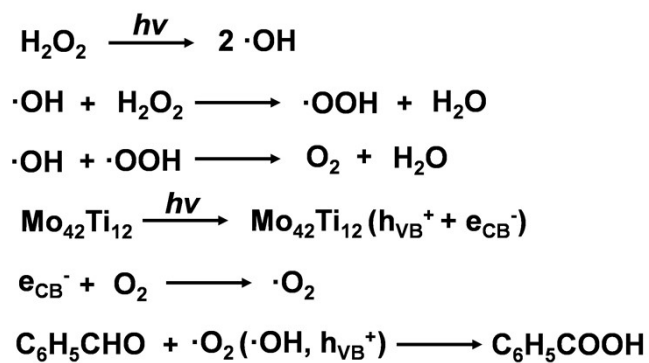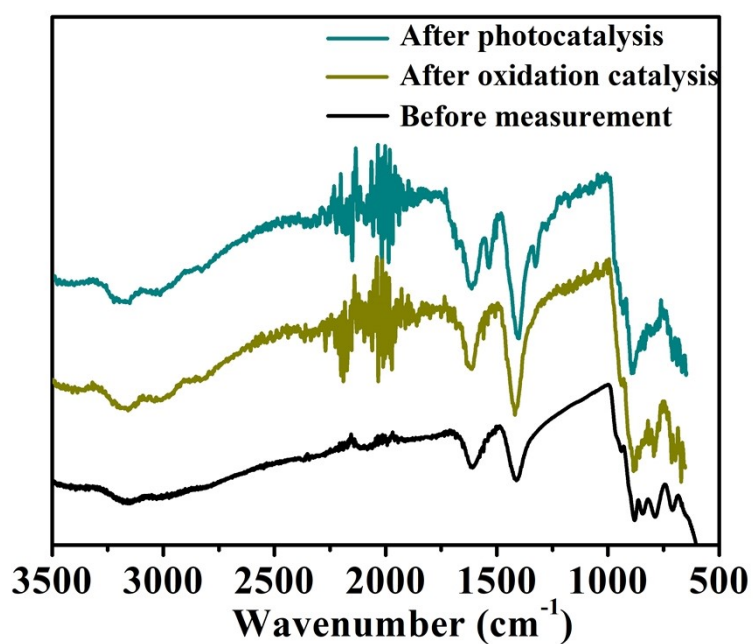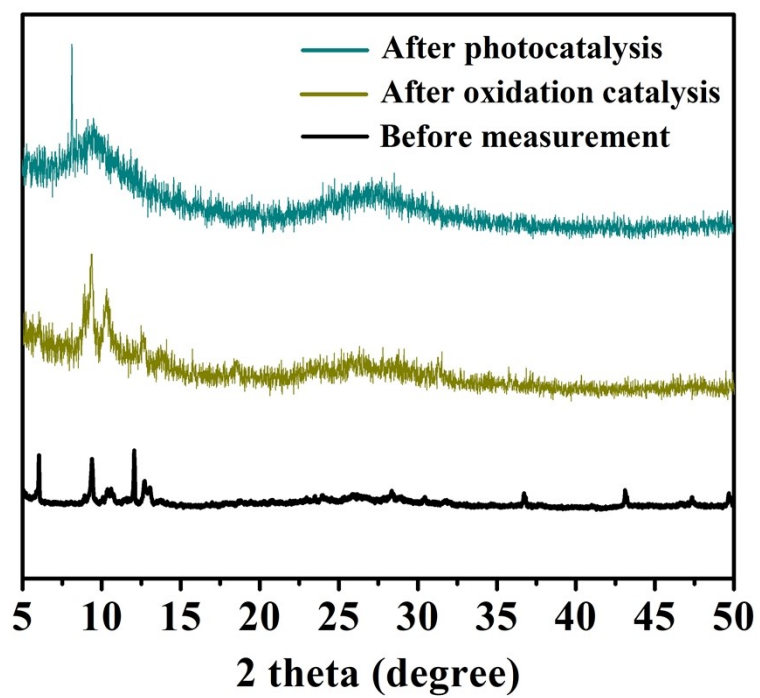| Compounds	MoTi	Nuclearity	Ref.
$[K_8(H_2O)_8][Ti_{12}(O_2)_6(OH)_{12}Mo_{42}O_{124}(O_2)_{18}(H_2O)_{17}]$	$Mo_{42}Ti_{12}$	54	this work
$[Mo_2Ti_2O_4(OMe)_6(O^iPr)_6]$	Mo_2Ti_2	4	9
$[Mo_6Ti_6O_{22}(OiPr)_{16}(iPrOH)_2]$	Mo_6Ti_6	12	9
$[(n-C_4H_9)_4N]_2[HCp*TiMo_5O_{18}]$	Mo_5Ti	6	10
$[Mo_4Ti_4O_{10}(OEt)_6(O^iPr)_8(BA)_2]$	Mo_4Ti_4	8	11
$[H_2Mo_4Ti_4(\mu_2-O)_6(\mu_3-O)_4Bz_{10}]$	Mo_4Ti_4	8	11
$[H_2Mo_4Ti_6(\mu_2-O)_6(\mu_3-O)_4Bz_{14}(OiPr)_4]$	Mo_4Ti_6	10	12
$[Mo^V_4Ti^{IV}_4O_{10}(OC_2H_5)_{14}(C_6H_5COO)_2]$	Mo_4Ti_4	8	13
$[Mo^V_4Mo^{VI}_2Ti^{IV}_4O_{16}(OCH_3)_{16}]$	Mo_6Ti_4	10	13
$[\{Mo_2Ti_4O_8(OEt)_{10}\}_2]$	Mo_4Ti_8	12	14

Table S2. Collected Examples of polyoxometalates build up by lacunary building blocks.

Lacunary building blocks	Compounds	Ref.
$[Mo_5(O_2)_2O_{17}]^{8-}$	$[Mo_{42}O_{124}(O_2)_{18}Ti_{12}(O_2)_6(OH)_{12}(H_2O)_{17}]^{8-}$	**This work**
$[PMo_9O_{34}]^{9-}$	$[\{PMo_9O_{34}TiO\}_2]^{14-}$	*Chem. Commun.*, 2020, **56**, 1097-1100 (Our previous work)
$[SiW_9O_{34}]^{10-}$	$Ag_{14}(DPPB)_4(CH_3CN)_9[Ag_{24}(Si_2W_{18}O_{66})_3]^{20-}$	*Angew. Chem. Int. Ed.*, 2024, **63**, e202317341
$[B-\alpha-SbW_9O_{33}]^{9-}$	$[Sb_{15}Tb_7W_3O_{29}(OH)_3(DMF)(H_2O)_6(SbW_8O_{30})(SbW_9O_{33})_5]^{27-}$	*Angew. Chem. Int. Ed.*, 2022, **61**, e202210019
$[A-\alpha-PW_9O_{34}]^{9-}$	$[\{(B-\alpha-PW_9O_{34})Co_3(OH)(H_2O)_2(O_3PC(O)(C_3H_6NH_3)PO_3)\}_2Co]^{14-}$	*Angew. Chem. Int. Ed.*, 2023, **62**, e202303290
$[A-\alpha-PMo_9O_{34}]^{9-}$	$[A-\alpha-PMo_9O_{31}(py)_3]_{3-}$	*Angew. Chem. Int. Ed.*, 2021, **60**, 6960-6964
$[SiW_9O_{34}]^{10-}$	$[Ag_7(Si_3W_{27}O_{96})]^{13-}$	*Angew. Chem. Int. Ed.*, 2020, **59**, 16361-16365
$[P_2W_{17}O_{61}]^{10-}$	$[P_2W_{17}O_{57}(PO_3C_{21}H_{14}N_3)(PO_4C_{24}H_{41})]^{10-}$	*Angew. Chem. Int. Ed.*, 2019, **58**, 18281-18285
$[Nb_7O_{22}]^{9-}$	$[Nb_{24}O_{72}H_8]^{16-}$	*J. Am. Chem. Soc.*, 2018, 140, **34**, 10803–10813
$[\alpha-P_2W_{15}O_{56}]^{12-}$	$[Co^{II}_9(H_2O)_6(OH)_3(p-RC_6H_4As^VO_3)_2(\alpha-P^V_2W^{VI}_{15}O_{56})_3]^{25-}$	*J. Am. Chem. Soc.*, 2017, **139**, 14501-14510
$[P_2W_{12}O_{48}]^{14-}$	$[\{\gamma-P_2W_{12}O_{48}Mn_4(acac)_2(OAc)\}_6]^{42-}$	*Angew. Chem. Int. Ed.*, 2016, **55**, 9630-9633
$[A-\alpha-GeW_9O_{34}]^{10-}$	$[Zr_{24}O_{22}(OH)_{10}(H_2O)_2(W_2O_{10}H)_2(GeW_9O_{34})_4(GeW_8O_{31})_2]^{32-}$	*J. Am. Chem. Soc.*, 2014, **136**, 7637−7642

[γ-SiW$_{10}$O$_{36}$]$^{8-}$	[{Zn(OH$_2$)(μ$_3$-OH)}$_2${Zn(OH$_2$)$_2$}$_2${γ-HSiW$_{10}$O$_{36}$}$_2$]$^{8-}$	*Angew. Chem. Int. Ed.*, 2010, **49**, 6096-6100
[α-PW$_{11}$O$_{39}$]$^{7-}$	[{(α-PW$_{11}$O$_{39}$H)Ln(H$_2$O)$_3$}$_2$]$^{6-}$	*Cryst. Growth Des.*, 2009, 9, **10**, 4362-4372

Table S3: Crystal data and structure refinement for **1**.

Empirical formula	Mo$_{42}$K$_8$O$_{209}$Ti$_{12}$H$_{62}$
Mr (g mol^{-1})	8323.57
Crystal system	monoclinic
Space group	P2$_1$/n
a/Å	17.3790(9)
b/Å	36.587(2)
c/Å	39.015(2)
α/°	90
β/°	93.9210(10)
γ/°	90
Volume/Å3	24750(2)
Z	4
ρcalcg/cm3	2.234
μ/mm-1	2.643
F(000)	15565.0
Radiation	Mo Kα (λ = 0.71073)
2Θ range for data collection/°	2.742 to 50.078
Independent reflections	43613 [Rint = 0.0727, Rsigma = 0.0796]
Goodness-of-fit on F2	1.019
Final R indexes [I>=2σ (I)]	R$_{1a}$ = 0.0811, wR$_{2b}$ = 0.2008
Final R indexes [all data]	R$_1$ = 0.1369, wR$_2$ = 0.2381

[a]$R_1 = \sum ||F_o| - |F_c|| / \sum |F_o|$, [b]$\omega R_2 = \{\sum \omega [(F_o)^2 - (F_c)^2]^2 / \sum \omega [(F_o)_2]^2\}^{1/2}$.

Table S4: BVS values for Mo atoms in **1**.
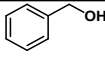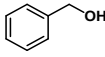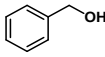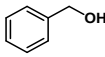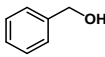
Molybdenum atom	BVS	Assigned Oxidation States
	Mo(VI)	
Mo1	6.054	VI
Mo2	6.064	VI
Mo3	6.077	VI
Mo4	5.903	VI
Mo5	6.156	VI
Mo6	5.550	VI
Mo7	5.598	VI
Mo8	5.776	VI
Mo9	5.411	VI
Mo10	6.030	VI
Mo11	5.720	VI
Mo12	5.716	VI
Mo13	5.450	VI
Mo14	5.552	VI
Mo15	5.687	VI
Mo16	6.074	VI
Mo17	6.413	VI
Mo18	5.486	VI
Mo19	6.085	VI
Mo20	6.033	VI
Mo21	6.147	VI
Mo22	5.937	VI
Mo23	6.089	VI
Mo24	5.472	VI
Mo25	6.098	VI
Mo26	5.729	VI
Mo27	5.674	VI
Mo28	5.659	VI
Mo29	6.152	VI
Mo30	6.308	VI
Mo31	5.772	VI
Mo32	5.370	VI
Mo33	5.682	VI
Mo34	6.188	VI
Mo35	6.287	VI
Mo36	6.270	VI
Mo37	6.086	VI
Mo38	5.924	VI

Mo39	6.355	VI
Mo40	5.588	VI
Mo41	5.528	VI
Mo42	5.550	VI

Table S5: BVS caculations for the Ti sites in **1**.

Titanium atom	BVS	Assigned Oxidation States
	Ti(IV)	
Ti1	4.130	IV
Ti2	4.430	IV
Ti3	4.439	IV
Ti4	4.400	IV
Ti5	4.337	IV
Ti6	4.340	IV
Ti7	4.429	IV
Ti8	4.389	IV
Ti9	4.474	IV
Ti10	4.309	IV
Ti11	4.426	IV
Ti12	4.455	IV
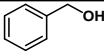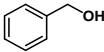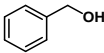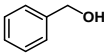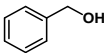
Table S6: Effect of time on the oxidative of benzyl alcohol.[a]

Catalysts	Substrate	T (°C)	Reaction time (h)	Conversions (%)[b]	Selectivities (%)[b]
1	C6H5CH2OH	65	12	99	91.5
1	C6H5CH2OH	65	24	99	96.4
1	C6H5CH2OH	65	36	99	96.8
1	C6H5CH2OH	65	48	99	90.1
1	C6H5CH2OH	65	60	99	92.1

[a] Reaction conditions: $Mo_{42}Ti_{12}$ (**1**) (3.0 mol%), benzyl alcohol (0.21 mmol), H_2O_2 (1.63 mmol), H_2O (3 mL),T (65 °C).

[b] Conversion and Selectivity were calculated from gas chromatography.

Table S7: Recycling experiments of catalyst.[a]

Catalysts	Substrate	T (°C)	Reaction time (h)	Run time	Conversions (%)[b]	Selectivities (%)[b]
1	(benzyl alcohol)	65	24	1	99	96.4
1	(benzyl alcohol)	65	24	2	99	95.9
1	(benzyl alcohol)	65	24	3	99	94.5
1	(benzyl alcohol)	65	24	4	99	93.6
1	(benzyl alcohol)	65	24	5	99	92.2

[a] Reaction conditions: $Mo_{42}Ti_{12}$ (**1**) (3.0 mol%), benzyl alcohol (0.21 mmol), H_2O_2 (1.63 mmol), H_2O (3 mL),T (65 °C), t (24 h).
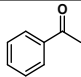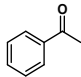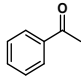
[b] Conversion and Selectivity were calculated from gas chromatography.

Table S8. A comparison of the oxidation of benzyl alcohol of **1** and those of some other representative POM, POM-based materials.

Catalyst	substrate	Oxidant	solvent	Light	T(°C)	t/h	Conv. (%)	BAD Sel.(%)	BZA Sel.(%)	Ref.
$Mo_{42}Ti_{12}$ (50mg)	BA (0.2mmol)	H_2O_2	H_2O	no	65	12/24	99	91.5/96.4	-	**This work**
$Mo_{42}Ti_{12}$ (5mg)	BAD (1mmol)	H_2O_2	H_2O	AM 1.5	55	12	92.6	-	>99	**This work**
$K_4[SiW_{12}O_{40}]$ (30mg)	BA (0.1mmol)	O_2	CH_2Cl_2	365nm	R.T.	12	40±5	99±1	-	15
$[Ag][Ag_4L_3][SiW_{12}]$ (30mg)	BA (0.1mmol)	O_2	CH_2Cl_2	365nm	R.T.	12	99±1	-	99±1	15
$Bi_4Ti_3O_{12}$ (10mg)	BA (0.1mmol)	O_2	BTF	>360nm	R.T.	5	35.5±5	99.8 ± 0.1	-	16
$[Ti_{19}Bi_2]$ (100mg)	BA (40umol)	O_2	MeCN	AM 1.5	R.T.	12	100	>99	-	17
$TMADT(W_{10}O_{32})$ (0.012mmol)	BA (1mmol)	O_2	MeCN	Vis	25	12	51.2	40.7	10.5	18
$[Cu_{1.5}(DPNDI)_{1.5}H_{1.5}P_2W_{18}O_{62}]$ (10mg)	BA (0.5mmol)	H_2O_2	EtOH/H_2O	white LED	R.T.	16	75	99	-	19
PMo_{12}-$ZnIn_2S_4$ (5mg)	BA (0.2mmol)	Ar	H_2O	$\lambda > 420$ nm	R.T.	5	96.1	98.2	-	20
[TBA-Q-Al] (20mg)	BA (0.5mmol)	O_2	MeCN	420-430nm	R.T.	24	100	-	>99	21
$[W_{10}O_{32}][Cp_3Zr_3]$ (1mol%)	BA (0.2mmol)	O_2	BTF	385nm	R.T.	12	97	>99	-	22

Catalyst	Substrate	Oxidant	Solvent	Light	Temp.	Time				Ref.
$ZnSiF_6PW_{12}$ (0.005mmol)	BA (1mmol)	Air	MeCN	320-780nm	R.T.	11	67	85	-	23
PW_{12}-PUCNS (20mg)	BA (0.1mmol)	O_2	H_2O	UV-Vis	20	2	58.3	99.5	-	24
$[Te_2Mo_{12}\{Ru(C_6H_6)\}]/\{PW_9\}/\{PMo_{12}\}/\{SiW_{12}\}$ (3mg)	BA (0.5mmol)	O_2	MeCN	white LED	R.T.	24	98/91/65/60	96/56/100/67	-	25
$CsPbBr_3/Ni_4P_2$-0.19 (10mg)	BA (0.05mmol)	O_2	MeCN	>400nm	R.T.	6	98	99	-	26
$Mg_2Al–Zn_4(PW_9)_2/$ K-$Zn_4(PW_9)_2$ (0.01mmol)	BA (1mmol)	H_2O_2	MeCN	-	60	6	95/ 100	13/ 92	-	27
HPW/AC-COIMI-HPW(5) (30mg)	BA (4mmol)	H_2O_2	MeCN/ H_2O	-	90	6	58.6/ 91.3	70.1/ 90.4	-	28
$(TBA)_5PMoV_2$ (100mg)	BA (0.01mol)	O_2	MeCN/ H_2O	-	170	4	93	>99	-	29
$[TMGHA]_{2.4}H_{0.6}PW$ (0.03mmol)	BA (10mmol)	H_2O_2	MeCN	-	90	6	69.8	91.8	-	30
HPW/ILPW/PIPA$_{13}$ (0.13mmol)	BA (10mmol)	H_2O_2	H_2O	-	95	6	48/59/96	67/80/86	-	31
$NH_2MIL_{88}B(Fe)$-PMo_{12} (20mg)	BA (1mmol)	TBHP	DMF	-	100	8	87	>99	-	32
APMo/49%APMo@Alrp (100mg)	BA (4mmol)	H_2O_2	MeCN	-	80	10	46/81	79/100	-	33
Im-PW/GO (600mg)	BA (40mmol)	H_2O_2	H_2O	-	90	7	90.1	99.2	-	34
$PMoV_2$@UiO-66-NH_2 (20 mg)	BA (1mmol)	H_2O_2	solvent-free	-	90	4	95	100	-	35
PTA@MMS (5umol)	BA (1mmol)	H_2O_2	MeCN	-	90	15	57.3	97	-	36
$\{[Cd(bix)_2][V^{IV}_8V^V_7]_2\}$ (0.005mmol)	BA (0.5mmol)	O_2	MeCN	-	120	10	>99	100	-	37
$[(CH_3)_3NC_{12}H_{25}]_2Na_5PW_{11}O_{39}$ (0.2mmol)	BA (10mmol)	H_2O_2	solvent-free	-	60	6	78.3	75.5	-	38
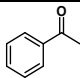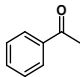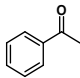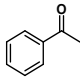
Table S9: The study of experimental mechanism.[a]

Entry	Substrate	Additive	Light	Conversions (%)[b]	Selectivities (%)[b]
1		isopropanol	AM 1.5G	87.6	99
2		Ammonium oxalate	AM 1.5G	89.3	99
3		1,4-benzoquinone	AM 1.5G	67.3	99

[a] Reaction conditions: $Mo_{42}Ti_{12}$ (**1**) (0.3 mol%), benzaldehyde (1 mmol), H_2O_2 (16.3 mmol), H_2O (3 mL),T (55 °C), t (12 h).

[b] Conversion and Selectivity were calculated from gas chromatography.

Table S10: Recycling experiments of catalyst.[a]

Catalysts	Substrate	T (°C)	Reaction time (h)	Run time	Conversions (%)[b]	Selectivities (%)[b]
1		55	12	1	92.6	99
1		55	12	2	92.4	99
1		55	12	3	91.5	99
1		55	12	4	91.2	99
1		55	12	5	90.2	99

[a] Reaction conditions: $Mo_{42}Ti_{12}$ (**1**) (0.3 mol%), benzaldehyde (1 mmol), H_2O_2 (16.3 mmol), H_2O (3 mL),T (55 °C), t (12 h).

[b] Conversion and Selectivity were calculated from gas chromatography.

Section S5 References

1. D. Leggas, O. V. Tsodikov, Determination of small crystal structures from a minimum set of diffraction intensities by homotopy continuation, *Acta Cryst. A.,* 2015, **71**, 319-324.

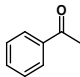2. A. Spek, PLATON SQUEEZE: a tool for the calculation of the disordered solvent contribution to the calculated structure factors, *Acta Cryst. C.,* 2015, **71**, 9-18.

3. A. Spek, Structure validation in chemical crystallography, *Acta Cryst. D.,* 2009, **65**, 148-155.

4. I. D. Brown, D. Altermatt, Bond-valence parameters obtained from a systematic analysis of the Inorganic Crystal Structure Database, *Acta Crystallogr. Sect. B.*, 1985, **41**, 244.

5. N. E. Brese, M. O'Keeffe, Bond-valence parameters for solids, *Acta Crystallogr. Sect. B.*, 1991, **47**, 192.

6. C. Wang, C. Liu, L. J. Li, Z. M. Sun, Synthesis, Crystal Structures, and Photochemical Properties of a Family

of Heterometallic Titanium Oxo Clusters, *Inorg. Chem*., 2019, **58**, 6312-6319.

7. Y. C. Yang, Q. X. Liu, Z. H. Zhou, H. L. Wan, Regioselective conversions of H_4pdta (1,2-propanediaminetetraacetic acid) and H_4eed3a to their triacetates on peroxotitanates, *Dalton Trans*., 2019, **48**, 16943.

8. A. Sundar, S. Bhattacharya, J. Oberstein, X. Ma, B. S. Bassil, T. Nisar, D. H. Taffa, M. Wark, V. Wagner, U. Kortz, Organically Functionalized Mixed-Valent Polyoxo-30-molybdate Wheel and Neutral Tetramolybdenum(V) Oxo Cluster, *Inorg. Chem*., 2022, **61**, 11524-11528.

9. H. Uchiyama, D. Puthusseri, J. Grins, D. Gribble, G. A. Seisenbaeva, V. G. Pol, V. G. Kessler, Single-Source Alkoxide Precursor Approach to Titanium Molybdate, $TiMoO_5$, and Its Structure, Electrochemical Properties, and Potential as an Anode Material for Alkali Metal Ion Batteries, *Inorg. Chem*., 2021, **60**, 3593-3603.

10. H. Akashi a , J. Chen b , H. Hasegawa c , M. Hashimoto d , T. Hashimoto c , T. Sakuraba c , A. Yagasaki, Synthesis and structural characterization of $[H_xCp^*TiMo_5O_{18}]^{(3-x)-}$ (x=0, 1, 2); new insights into protonation patterns in polyoxometalates, *Polyhedron*, 2003, **22**, 2847-2854.

11. L. Yang, X. P. Shu, M. Y. Fu, H. Y. Wang, Qi. Y. Zhu, J. Dai, Molybdenum–titanium oxo-cluster, an efficient electrochemical catalyst for the facile preparation of black titanium dioxide film, *Dalton Trans*., 2020, **49**, 10516-10522.

12. D. X. Wang, Y. S. Liu, G. J. Chen, F. F. Gao, G. Y. Zhang, G. Wang, C. H. Tung, Y. F. Wang, Ligation of Titanium-oxide and {Mo_2} Units for Solar CO_2 Storage, *Inorg. Chem*., 2023, **62**, 21074-21082.

13. W. Z Chen, X. F. Yi, J. Zhang, L. Zhang, Heterometallic Mo–Ti oxo clusters with metal–metal bonds: Preparation and visible-light absorption behaviors, *Polyoxometalates*, 2023, **2**, 9140013.

14. S. Eslava, B. P. R. Goodwill, M. McPartlin, D. S. Wright, Extending the Family of Titanium Heterometallic–oxo–alkoxy Cages, *Inorg. Chem*., 2011, **50**, 5655-5662.

15. S. M. Zhang, Y. Wang, Y. Y. Ma, Z. B. Li, J. Du, Z. G. Han, Three-Dimensional Silver-Containing Polyoxotungstate Frameworks for Photocatalytic Aerobic Oxidation of Benzyl Alcohol, *Inorg. Chem*., 2022, **61**, 20596-20607.

16. M. C. Shen, Y. Z. Shi, Z. W. Wang, T. K. Wu, L. Hu, L. Wu, Enhanced photocatalytic benzyl alcohol oxidation over $Bi_4Ti_3O_{12}$ ultrathin nanosheets, *J. Colloid Interface Sci*., 2022, **608**, 2529-2538.

17. C. Y. Liu, H. H. Niu, D. X. Wang, Y. S. Liu, A. Said, G. Wang, C. H. Tung, Y. F. Wang, Bi-Doped Ti-Oxide Cluster Photocatalyst with High Performance in the Selective Transformation of Benzyl Alcohols to Benzaldehydes, *Cryst. Growth Des*., 2023, **23**, 6866-6875.

18. B. Yang, Z. H. Fu, A. Q. Su, J. L. She, M. K. Chen, S. P. Tang, W. W. Hu, C. Zhang, Y. C. Liu, Influence of tetraalkylammonium cations on quality of decatungstate and its photocatalytic property in visible light-triggered selective oxidation of organic compounds by dioxygens, *Appl. Catal. B Environ. Energy*, 2019, **242**, 249-257.

19. C. Si, X. L. Liu, T. Zhang, J. B. Xu, J. Li, J. Y. Fu, Q. X. Han, Constructing a Photocatalyst for Selective Oxidation of Benzyl Alcohol to Benzaldehyde by Photo-Fenton-like Catalysis, *Inorg. Chem*., 2023, **62**, 4210-4219.

20. F. S. Xing, R. Y. Zeng, C. C. Cheng, Q. W. Liu, C. J. Huang, POM-incorporated $ZnIn_2S_4$ Z-scheme dual-functional photocatalysts for cooperative benzyl alcohol oxidation and H_2 evolution in aqueous solution, *Appl. Catal. B Environ. Energy*, 2022, **306**, 121087.

21. S. Ru, C. C. Zhao, Z. K. Wu, L. K. Yan, D. J. Zang, Y. G. Wei, Molecular Photocatalysts Based on Quinolinium-Grafted Polyoxometalates for Efficient One-Step Aerobic Oxidation of Benzyl Alcohols to Benzoic Acids, *ACS Sustainable Chem. Eng.*, doi.org/10.1021/acssuschemeng.3c05573.

22. Q. X. Gu, X. L. Zhao, M. Meng, Z. Y. Shao, Q. Zheng, W. M. Xuan, Crystalline porous ionic salts assembled from polyoxometalates and cationic capsule for the selective photocatalytic aerobic oxidation of aromatic alcohols to aldehydes, *Chin. Chem. Lett.*, 2023, **34**, 107444.

23. J. Z. Liao, H. L. Zhang, S. S. Wang, J. P. Yong, X. Y. Wu, R. M. Yu, C. Z. Lu, Multifunctional Radical-Doped Polyoxometalate-Based Host–Guest Material: Photochromism and Photocatalytic Activity, *Inorg. Chem.*, 2015, **54**, 4345-4350.

24. L. F. Wu, S. An, Y. F. Song, Heteropolyacids-Immobilized Graphitic Carbon Nitride: Highly Efficient Photo-Oxidation of Benzyl Alcohol in the Aqueous Phase, *Engineering*, 2021, **7**, 94-402.

25. W. Tang, Y. N. Liu, Y. Z. Jin, W. X. Shi, J. L. Sun, P. T. Ma, J. Y. Niu, J. P. Wang, $\{Ru(C_6H_6)\}$-Decorating Heteropolymolybdate for Highly Activity Photocatalytic Oxidation of Benzyl Alcohol to Benzaldehyde, *Chem. Eur. J.*, 2024, **30**, e202302921.

26. Y. Y. Dong, Y. Q. Feng, Z. Li, H. Zhou, H. J. Lv, G. Y. Yang, $CsPbBr_3$/Polyoxometalate Composites for Selective Photocatalytic Oxidation of Benzyl Alcohol, *ACS Catal.*, 2023, **13**, 14346-14355.

27. K. Liu, Y. Q. Xu, Z. X. Yao, H. N. Miras, Y. F. Song, Polyoxometalate-Intercalated Layered Double Hydroxides as Efficient and Recyclable Bifunctional Catalysts for Cascade Reactions, *ChemCatChem.*, 2016, **8**, 929-937.

28. M. Zheng, H. T. He, X. Z. Li, D. L. Yin, Imidazolized Activated Carbon Anchoring Phosphotungstic Acid as a Recyclable Catalyst for Oxidation of Alcohols With Aqueous Hydrogen Peroxide, *Front. Chem.*, 2022, **10**, 925622.

29. J. Díaz, L. R. Pizzio, G. Pecchi, C. H. Campos, L. Azócar, R. Briones, R. Romero, A. Henríquez, E. M. Gaigneaux, D. Contreras, Tetrabutyl Ammonium Salts of Keggin-Type Vanadium-Substituted Phosphomolybdates and Phosphotungstates for Selective Aerobic Catalytic Oxidation of Benzyl Alcohol, *Catalysts*, 2022, **12**, 507.

30. G. J. Chen, Y. Zhou, Z. Y. Long, X. C. Wang, J. Li, J. Wang, Mesoporous Polyoxometalate-Based Ionic Hybrid As a Triphasic Catalyst for Oxidation of Benzyl Alcohol with H_2O_2 on Water, *ACS Appl. Mater. Interfaces*, 2014, **6**, 4438-4446.

31. P. B. Hao, M. J. Zhang, W. Zhang, Z. Y. Tang, N. Luo, R. Tan, D. H. Yin, Polyoxometalate-based Gemini ionic catalysts for selective oxidation of benzyl alcohol with hydrogen peroxide in water, *Catal. Sci. Technol.*, 2018, **8**, 4463-4473.

32. M. Mohammadikish, M. Panahi, An Fe·MOF–Mo·POM hybrid material: a novel and efficient catalyst for selective benzyl alcohol oxidation to benzaldehyde, *CrystEngComm.*, 2023, **25**, 5470-5478.

33. L. H. Wang, S. X. Ma, C. H. Chen, B. Lu, Z. Wang, Y. Wang, S. J. Mao, Pentacoordinated Al^{3+} stabilized polyoxometalates for the efficient catalytic valorization of biomass-derived feedstocks, *Catal. Sci. Technol*., 2023, **13**, 3558-3567.

34. W. H. Zhang, J. J. Shen, J. Wu, X. Y. Liang, J. Xu, P. Liu, B. Xue, Y. X. Li, An amphiphilic graphene oxide-immobilized polyoxometalate-based ionic liquid: A highly efficient triphase transfer catalyst for the selective oxidation of alcohols with aqueous H_2O_2, *Mol. Catal*., 2017, **443**, 262-269.

35. K. M. Ahmed, K. Amani, A novel amine-functionalized polyoxometalate-based metal-organic framework: A reusable heterogeneous nanocomposite for selective oxidation of alcohols, *J. Mol. Struct*., 2024, **1303**, 137503.

36. R. Chilivery, V. Chaitanya, J. Nayak, S. Seth, R. K. Rana, Heterogenization of Phosphotungstate Clusters into Magnetic Microspheres: Catalyst for Selective Oxidation of Alcohol in Water, *ACS Sustainable Chem. Eng*., 2022, **10**, 6925-6933.

37. H. R. Tian, R. H. Li, J. Miao, S. X. Liu, F. F. Wang, Z. P. Zheng, Additive-free selective oxidation of aromatic alcohols with molecular oxygen catalyzed by a mixed-valence polyoxovanadate-based metal–organic framework, *Dalton Trans*., 2023, **52**, 9121-9130.

38. F. L. Yu, M. X. Liu, B. Yuan, C. X. Xie, S. T. Yu, Selective Oxidation of Primary Alcohols to Carboxylic Acids Using Lacunary Polyoxometalates Catalysts and Hydrogen Peroxide, *Catal. Lett*., 2023, **153**, 1738-1742.